## PAPER

# A green approach for enhancing the hydrophobicity of UiO-66(Zr) catalysts for biodiesel production at 298 K†

Ahmed S. Abou-Elyazed, [ab] Yinyong Sun, [*a] Ahmed M. El-Nahas [*b] and Ahmed M. Yousif[bc]

Recently, the incorporation of hydrophobicity on the surface of UiO-66(Zr) has received much attention due to the deactivation of hydrophilic active sites of UiO-66(Zr) upon water adsorption. In this work, we report UiO-66(Zr) catalysts with an assortment of surface hydrophobicities fabricated by the solvent-free method to elucidate the impact of the environment framing Lewis acid sites on their catalytic activity in the production of fatty acid methyl ester (biodiesel) *via* the esterification of fatty acids at room temperature with high selectivity (100%) and good recyclability. A detailed structural analysis of the materials by $N_2$ sorption, FT-IR, SEM, XRD, water contact angle measurement, dynamic liquid scattering (DLS), NMR and TGA revealed the fabrication of stearic acid-grafted UiO-66(Zr) catalysts (10SA/UiO-66) with fine particle size and a highly hydrophobic network. 10SA/UiO-66(Zr) with enhanced hydrophobicity exhibited superior catalytic performance in the esterification of a fatty acid with a long alkyl chain compared with conventional solid acid catalysts and even liquid acid catalysts. Detailed kinetic studies corroborated that the adsorption of lipophilic acids at the Lewis acid sites besides the enhancement of wettability between the reactants was facilitated by the hydrophobic environment, thus significantly motivating the esterification reaction at room temperature. Furthermore, 10SA/UiO-66(Zr) showed good catalytic activity in the esterification of oleic acid in the presence of water (~10% in the light of acid weight).

## 1. Introduction

The dependence of the world on fuel has reached notable levels. It is necessary to find alternative sources of renewable energy, such as solar energy, wind energy, hydroelectric energy and biofuel energy, in order to increase the energy security of the world.[1] Therefore, renewable fuels are an ideal way to solve this serious problem. Biofuels obtained from biomass are considered to be one of the most promising renewable sources of energy.[2] They are characterized by the absence of toxic oxides ($CO_2$, $SO_x$) and thus limit the process of global warming, air pollution, and acid rains. In general, they have reduced health risks compared to fossil fuels.[3–5]

One of the most significant forms of biofuel is biodiesel, which is produced by the transesterification of vegetable oils/animal fats or fatty acids with small-molecular-weight alcohols, such as methanol and ethanol; methanol is the most widely utilized in this type of reaction owing to its strong nucleophilicity and low price.[6] Methanolysis reactions of vegetable oils or fatty acids occur in the existence of homogenous catalysts, which can be basic, acidic or an enzyme.[7–10] Homogenous base and acid catalysts are common in the industrial production of biodiesel as they have a high ability to accelerate the reaction under mild conditions and are less energy-intensive. However, there are some difficulties that limit the utilization of homogeneous base catalysts, including the difficulty in their separation from the reaction mixture,[11] in addition to the need for a large quantity of water to compensate and refine the products.[12] Economically, they increase biodiesel production costs.

Recently, heterogeneous catalysts have been introduced to solve the aforementioned problems because of their many advantages, including easy separation from the reaction mixture, environmental friendliness and good reusability.[13,14] Various types of heterogeneous catalysts, such as ion-exchange resins,[15] alkoxides,[16,17] Mg–Al hydrotalcites,[18–20] metal oxides and hydroxides,[21–24] are used in biodiesel production by the

[a]*MIIT Key Laboratory of Critical Materials Technology for New Energy Conversion and Storage, School of Chemistry and Chemical Engineering, Harbin Institute of Technology, Harbin, 150001, China. E-mail: yysun@hit.edu.cn; Tel: +86-45186413708*

[b]*Chemistry Department, Faculty of Science, Menoufia University, Shebin El-Kom, Egypt. E-mail: amelnahas@hotmail.com; Tel: +20 1064607974*

[c]*Chemistry Department, College of Science and Arts, Jouf University, Alqurayyat, Kingdom of Saudi Arabia*

alcoholysis of vegetable oils, animal fats or various fatty acids. Heterogeneous base catalysts are more efficient in activating the reaction than acid catalysts. However, the crude oils contain higher free fatty acids (FFAs) and water, which largely decrease the catalytic activity and reusability of the base catalysts as a result of soap formation and deactivation of active sites.[25] In contrast, acid catalysts can promote both esterification of free fatty acids (FFAs) and transesterification of triglycerides with alcohol, even in the presence of a little amount of water.[26] A high percentage of water that is present in the crude oil or produced as a byproduct from the reaction may be adsorbed on the catalysts due to the unique hydrophilic nature of the acidic sites on their surface and then cause the deactivation of the catalytic sites or hydrolysis of the frameworks.[27–29] In addition, many metal-based Lewis acids tend to decompose into metal hydroxides in water-containing environments.[30] Therefore, the development of solid acids with appropriate hydrophobicity can largely overcome these issues and upgrade the catalytic activity and reusability.

It is well-known that UiO-66(Zr) is a metal–organic framework (MOFs) that shows exceptional stability, high activity and excellent reusability in various organic reactions.[31,32] These features allow its use in a wide scope of thermal and chemical conditions. To the best of our knowledge, the key to their stability is the high topological connectivity of the $[Zr_6O_4(OH)_4]^{12+}$ secondary building unit (SBU), which is attached through the strong Zr–O bonds to 12 terephthalate (BDC) linkers. Thus, defects are created in the structure of UiO-66(Zr) when one or more linkers are replaced or removed from the crystalline network.[33] Experimentally, these defects are responsible for the enhancement in the catalytic activity of UiO-66(Zr) in various organic reactions,[34,35] since losing one or more linkers may introduce coordinately unsaturated Zr sites in the solid, resulting in the enrichment of open Lewis acid sites.

To date, most of the porous solid acid catalysts are hydrophilic owing to the hydrophilic nature of their frameworks and the acidic sites on their surfaces. Although some organic frameworks, such as carbonaceous materials, are naturally hydrophobic.[36,37] Water, a typical byproduct and the negative component of acid-catalyzed reactions, coadsorbs on the surface of hydrophilic solid acids, causing partial deactivation of the acidic sites and hydrolysis of the frameworks in some cases.[38] Recently, numerous investigations have been done on the fabrication of solid acid catalysts with a hydrophobic environment surrounding the active sites in the catalysts, which facilitate the adsorption of oleophilic materials and desorption of hydrophilic materials, such as water, on their surface. For instance, Chen and coworkers reported Pt@UiO-66@GO/rGO as a solid hydrophobic catalyst for the hydrogenation of nitrobenzene and *p*-nitrophenol into corresponding amino derivatives.[39] Further, Du and coworkers immobilized *Aspergillus niger* lipase (ANL) on hydrophobic UiO-66-PDMS to form a solid catalyst for biodiesel production.[40]

Inspired by the previous efforts, we prepared UiO-66(Zr) with defects and enhanced the hydrophobic environment around the active sites by grafting a saturated fatty acid (stearic acid) using a one-pot and solvent-free method. This promoted the hydrophobicity of the UiO-66(Zr) network without decreasing the reactivity of the zirconium sites. Thus, this facile and low-cost strategy can be widely applied with other types of MOFs and in other fields of heterogeneous catalysts to achieve a highly active acid catalyst for biomass conversion.

## 2. Experimental procedures

### 2.1. Materials

All chemicals were used directly as received: zirconyl chloride octahydrate ($ZrOCl_2 \cdot 8H_2O$), 1,4-benzenedicarboxylic acid (BDC), stearic acid (Tianjin Guangfu, 98%), MIL-100(Fe) (Tianjin Guangfu), ZMS-5 (Tianjin Guangfu), bentonite (Innochem, 98%), levulinic acid (Innochem, 98%), oleic acid (Tianjin Zhi Yuan, 98%), acetic acid (Sinopharm, 99.5%), methanol (Sinopharm, 99.7%), ethanol (Sinopharm, 99%), ethyl acetate (Aladdin, 99.5%), toluene (Sinopharm, 99.5%) and potassium hydroxide (Sinopharm, 99.5%).

### 2.2. Catalyst preparation

Stearic acid-grafted UiO-66(Zr) was synthesized by a green method; $ZrOCl_2 \cdot 8H_2O$ (1.5 mmol) as the metal precursor, 1,4-benzenedicarboxylic acid (BDC) as the organic linker (1.5 mmol) and 10% of stearic acid (according to the weight of the BDC linker) were ground together for about 10 min at room temperature. Then, the powder was moved into an autoclave at 130 °C for 24 h. After cooling to room temperature, the obtained white solid was washed with 70 °C ethanol and dried for 24 h at 150 °C under vacuum, as stated in the previous work.[41] The catalyst was referred to as 10SA/UiO-66(Zr).

Moreover, UiO-66(Zr)-green was synthesized as described in the literature,[42] and stearic acid-grafted UiO-66(Zr) was prepared by a solvothermal method, as described below: $ZrOCl_2 \cdot 8H_2O$ (1.5 mmol) as the metal precursor, BDC as the organic linker (1.5 mmol) and 10% stearic acid based on the weight of BDC were dissolved together in 25 mL DMF in a Teflon-lined stainless-steel autoclave at room temperature. The obtained homogeneous mixture was closed and placed in a pre-heated oven for 24 h at 130 °C. After cooling to room temperature, the resulting gel was washed with 70 °C ethanol and soaked in $CH_2Cl_2$ for 2 days and then centrifuged and dried for 24 h at 150 °C under vacuum. The catalyst was referred to as 10SA/UiO-66(Zr)-solvent.

### 2.3. Characterization of the formed catalyst

All the prepared samples were characterized using different techniques, such as BET, FT-IR, powder-XRD, SEM-EDX, NMR and TGA.

Brunauer–Emmett–Teller (BET) and Barret–Joyner–Halenda (BJH) methods were used to estimate the surface area and pore volume. The nitrogen sorption isotherms were recorded at −196 °C on a 3H-2000PS1 Gas Sorption and Porosimetry system for determining the surface area and pore characteristics. The samples were regularly arranged for examination after

degassing at 150 °C under vacuum until the final pressure reached $1 \times 10^{-3}$ torr.

The acidity of the UiO-66(Zr) samples was recorded with and without stearic acid incorporation. All the samples were activated by degassing for 2 h at 150 °C, then cooled under vacuum and saturated with liquid pyridine. The samples were again heated to 150 °C to liberate the physisorbed pyridine. The FTIR spectra were recorded with the KBr-pellet technique using a Bruker Equinox 55 Fourier transform infrared spectrophotometer, and the diffuse reflectance spectra were scanned over the range of 1000–1800 cm$^{-1}$ with a resolution (2 cm$^{-1}$) of 100 scans per measurement.

The XRD patterns were obtained on a Rigaku D/Max-2550 diffractometer furnished with a SolX detector and Cu Kα radiation with $\lambda$ = 1.5418 Å. The data were recorded with step scanning at $2\theta = 0.02°$ per second from 5° to 50°. The influence of stearic acid on the crystallinity and particle size of UiO-66(Zr) were investigated by using the crystallinity degree and Scherrer equations, respectively, as seen below:

$$\text{Crystallinity} = \frac{\text{area of crystalline peaks}}{\text{area of all peaks (crystalline + amorphous)}} \times 100 \quad (1)$$

$$D = \frac{k\lambda}{\beta \cos \theta} \quad (2)$$

where $D$, $k$, $\lambda$, $\beta$ and $\theta$ are the crystallite size (nm), Scherrer constant (0.9), wavelength (1.5418 nm), the full width at half-maximum-height of the peak FWHM (radian) and the peak position (radian), respectively.

The scanning electron microscopy (SEM) images were recorded on a SUPRA 55 at an acceleration voltage of 20 kV.

Dynamic light scattering (DLS) was performed with an ALV-5000/E DLS instrument (Malvern Instruments, U.K.) at a fixed scattering angle of 90° after filtering the samples through 0.45 μm Millipore filters.

The $^1$H NMR spectra were recorded on a Bruker Advance 400 MHz spectrometer with a digested deuterated mixture as the solvent at room temperature; the chemical shifts ($\delta$) are expressed in ppm.

The thermogravimetric analysis (TGA) was conducted on a Shimadzu TA-50. The Fourier transform infrared (FT-IR) spectra were acquired on a NicoLET iS10 spectrometer.

The water contact angles were measured with a CAST V2.6 (Solon Tech. Shanghai Co., Ltd., China). The volume of the water droplet was fixed at 3.0 μL, and the contact angle was estimated at 30 s after attachment to the material surface.
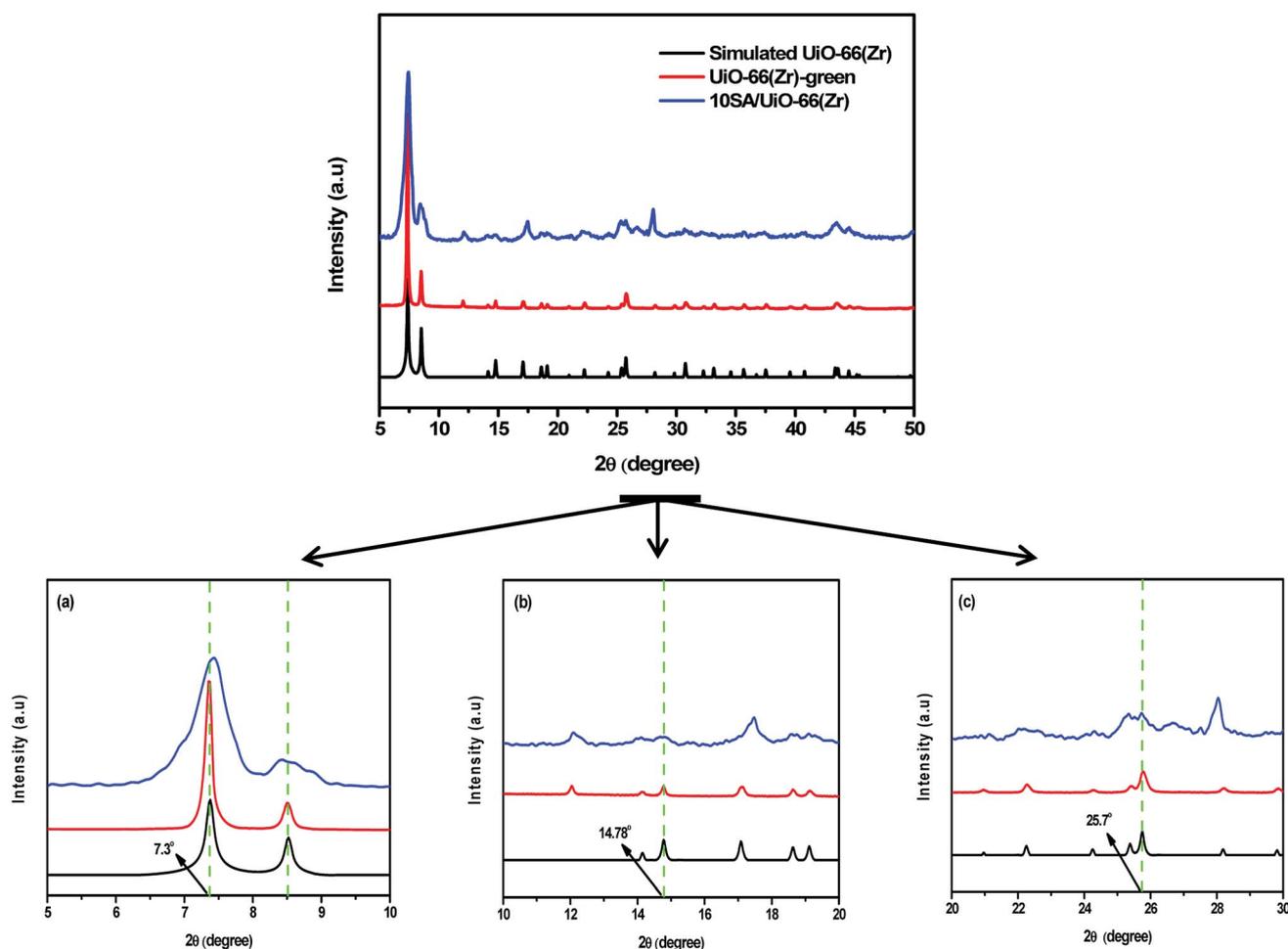


Fig. 1 XRD patterns of the samples: (a)–(c) are the magnifications of the local XRD patterns in different $2\theta$ ranges.

### 2.4. Calculation of the acid site density

This was performed with 50 mg of each catalyst after pretreatment at 150 °C for 2 h in the air before exposure to the probe molecule (pyridine). 15–20 mg of pyridine-covered samples were subjected to heating up to 150 °C for 2 h under vacuum. The mass loss because of pyridine desorption from the acidic sites was computed as a function of the total surface acidity at the sites (g$^{-1}$). The equation used to compute the acid site density is as follows:[43]

$$\text{Acid site density} =$$

$$\frac{\text{moles of pyridine adsorbed} \times \text{Avogdro's number (sites per mol)}}{\text{wt of catalyst(g)} \times \text{BET(m}^2 \text{ g}^{-1})} \tag{3}$$

### 2.5. Catalyst activity

The esterification reactions of oleic acid (fatty acid) with methanol to form methyl oleate (biodiesel) were performed in a batch reactor at 298 K, where 1 mmol of acid and 39 mmol of methanol were brought in contact with the catalyst (6% of the weight of acid), according to previous work.[42] After esterification, the catalyst was separated from the reaction medium by filtration and reused in the next esterification run. The conversion of oleic acid was determined using 0.1 M alcoholic KOH as the titrant in the presence of phenolphthalein as the indicator. The volume of KOH consumed was noted; the conversion of free fatty acid (FFA) and the product selectivity were estimated using eqn (4) and (5). The biodiesel was also quantitatively analyzed by gas chromatography on an Agilent 7890A GC with an FID detector, and the detailed outcomes were consistent with a standard deviation of ±0.01–0.025 mass%. All data are from triplicate experiments.

$$\% \text{ Conversion} = \frac{a_i - a_f}{a_i} \times 100 \tag{4}$$

$$\% \text{ Selectivity} = \frac{a_j}{a_i - a_f} \times 100 \tag{5}$$

where $a_i$, $a_f$, $a_j$ are the initial and final concentrations of the sample and the molar concentration of the product, respectively.

## 3. Results and discussion

### 3.1. Structural characterization

The structural integrity of UiO-66(Zr)-green and 10SA/UiO-66(Zr) was examined by XRD, as shown in Fig. 1. The peaks of 10SA/UiO-66(Zr) were in good agreement with the characteristic peaks of pristine UiO-66(Zr), which revealed that the crystal structure of UiO-66(Zr) was well maintained. However, the differences in the peak intensity in the diffractogram of 10SA/UiO-66(Zr) compared with that of UiO-66(Zr) suggested a change in the crystallinity degree and particle sizes due to the incorporation of stearic acid, as presented in Table S1.†

As seen in Fig. 1, the crystallinity slightly decreased, and stearic acid assisted the formation of UiO-66(Zr) with smaller
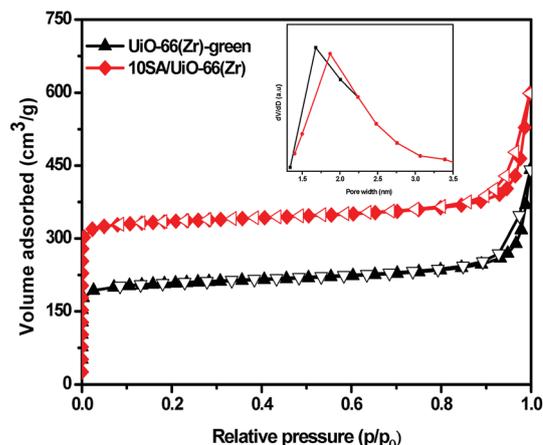


**Fig. 2** The N$_2$ sorption isotherms and pore distribution curves (inset) of the samples.

particle sizes. These results match well with those from the SEM and DLS analyses. Undoubtedly, the addition of stearic acid influenced the coordination between the Zr component and the organic linker.

The N$_2$ sorption results of the UiO-66(Zr)-green and 10SA/UiO-66(Zr) samples are shown in Fig. 2. The samples UiO-66(Zr)-green and 10SA/UiO-66(Zr) exhibited type I isotherms at relatively low pressure, indicating the presence of micropores. Additionally, the adsorption data listed in (Table S2†) reveal that 10SA/UiO-66(Zr) possessed a higher BET surface area (1150 m$^2$ g$^{-1}$) and pore volume (0.92 cm$^3$ g$^{-1}$) than those of UiO-66(Zr)-green (701 m$^2$ g$^{-1}$, 0.68 m$^3$ g$^{-1}$), suggesting that stearic acid had grafted into the framework of UiO-66(Zr) and did not accumulate inside the pores of UiO-66(Zr).

The FT-IR spectra of stearic acid (SA), UiO-66(Zr)-green and 10SA/UiO-66(Zr) were used to characterize the functional groups on the organic linkers in the prepared materials and to elucidate the interaction between stearic acid and the zirconium ions in the UiO-66(Zr) matrix. As shown in Fig. 3, the FT-IR spectrum of stearic acid (SA) showed peaks centered around
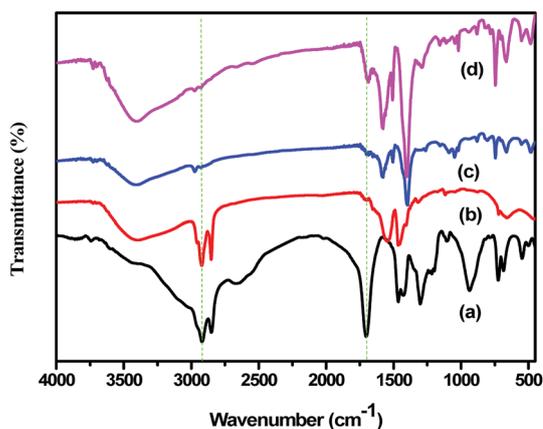


**Fig. 3** FT-IR spectra of (a) stearic acid, (b) Zr-stearate, (c) UiO-66(Zr)-green and (d) 10SA/UiO-66(Zr).
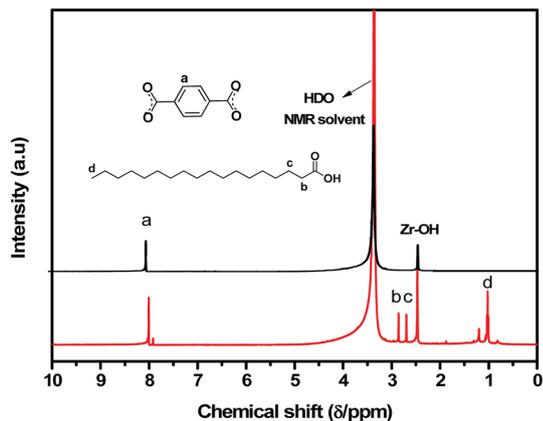
**Fig. 4** $^1$H NMR spectra of the UiO-66(Zr)-green and 10SA/UiO-66(Zr) samples.

2830 cm$^{-1}$ and 2920 cm$^{-1}$, which were assigned to the stretching vibrations of the CH$_2$-groups (Fig. 3a). Moreover, the peak located at around 1700 cm$^{-1}$ belonged to the stretching vibration of the carbonyl group from stearic acid, which overlapped with the carbonyl group of the BDC linker and gave two new characteristic peaks at 1480 and 1600 cm$^{-1}$ with high intensities (Fig. 3d). Moreover, the disappearance of the characteristic peak at 1670 cm$^{-1}$ corresponding to stearic acid indicated that chemical interaction between stearic acid and zirconium ions had occurred.[44,45] Notably, the FT-IR spectra of UiO-66(Zr) and 10SA/UiO-66(Zr) (Fig. 3c and d) exhibited a strong and broad band centered at 3440 cm$^{-1}$ due to the condensation of crystalline and physisorbed water inside the cavities.[46]

The organic components (*e.g.*, BDC, stearic acid) were identified by $^1$H liquid NMR spectroscopy. As seen in Fig. 4, there were only distinct resonance signals, which could be confidently assigned to the BDC-linker, Zr–OH and stearic acid. This is an early indication that stearic acid (SA) indeed compensates for the defects in the UiO-66(Zr) framework. However, it is of extreme significance to ascertain whether stearic acid (SA) is actually grafted into the UiO-66(Zr) framework or simply trapped in the pores as a free acid. We washed and activated the samples before the NMR analysis to confirm that all stearic acid (SA) molecules were successfully removed from the pores of

UiO-66(Zr). Therefore, we are confident that the stearic acid peaks revealed by the NMR analysis after activation arise from the molecules grafted into the UiO-66 framework.

The SEM images of the UiO-66(Zr)-green and 10SA/UiO-66(Zr) samples are displayed in Fig. 5. Both samples illustrated the same morphology but different crystal sizes. UiO-66(Zr)-green seemed to have an irregular morphology with a crystal size of around 200 nm (Fig. 5a), while 10SA/UiO-66(Zr) exhibited irregular shape and crystal sizes below 150 nm (Fig. 5b). This indicates the introduction of stearic acid had an inhibition effect on the crystal growth of UiO-66(Zr), which could explain the reason why the surface area and pore volume of UiO-66(Zr) were increased after the addition of stearic acid.

Further, the dynamic liquid scattering curves proved that 10SA/UiO-66(Zr) possessed a smaller particle size than UiO-66(Zr)-green (Fig. 6).

Additionally, the SEM images were simulated to display the surface roughness of UiO-66(Zr)-green and 10SA/UiO-66(Zr) using the Image J software. Fig. S1† shows the surface roughness plot and particle size distribution of both samples. Notably, the surface roughness value for 10SA/UiO-66(Zr) was higher than that for UiO-66(Zr)-green (more than 35%) (Fig. S2†), suggesting that possibly stearic acid has an effect on the wettability of the material.

The results from the thermogravimetric analysis indicated that 10SA/UiO-66(Zr) possessed high thermal stability similar to
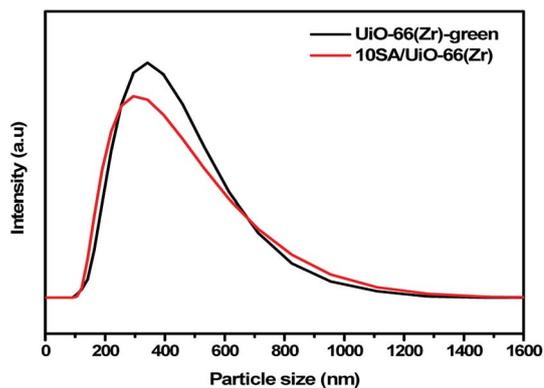


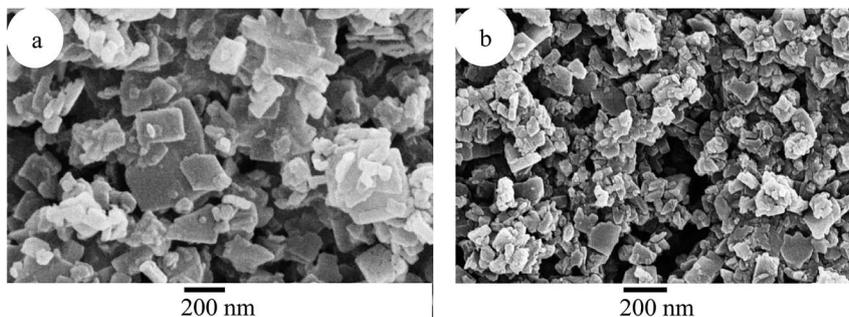**Fig. 6** The dynamic liquid scattering (DLS) curves of UiO-66(Zr)-green and 10SA/UiO-66(Zr).



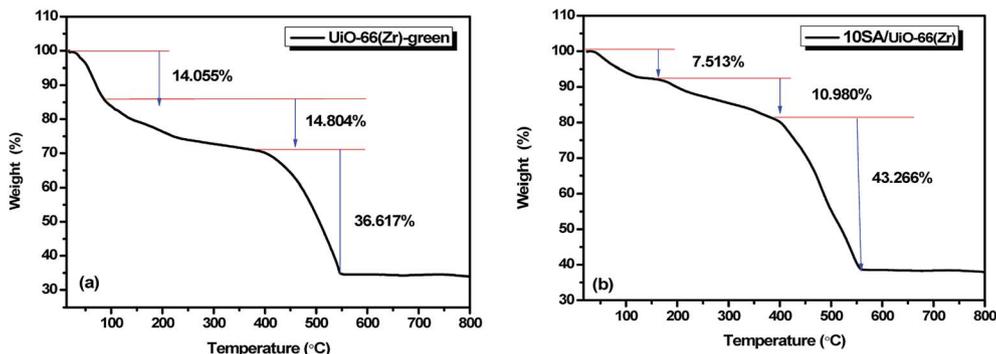**Fig. 5** SEM images of (a) UiO-66(Zr)-green and (b) 10SA/UiO-66(Zr).

Fig. 7 TGA curves of (a) UiO-66(Zr)-green and (b) 10SA/UiO-66(Zr).

UiO-66(Zr) prepared *via* green and conventional methods.[41] In Fig. 7, two distinct weight-loss regions can be identified for UiO-66(Zr); the first one before 400 °C could be assigned to the removal of adsorbed water from different sites. The second one above 400 °C resulted from the decomposition of the framework. In the case of 10SA/UiO-66(Zr), the initial weight-loss occurring in the temperature range of 25–90 °C was due to the removal of physisorbed water, whereas the second weight-loss observed in the temperature range of 90–235 °C was related to the removal of the aliphatic chain of stearic acid and

the dehydroxylation of the zirconium oxo-clusters. The third weight-loss above 400 °C was attributed to the decomposition of UiO-66 as a result of the burning of organic linkers (BDC and stearic acid) in the framework.

Interestingly, to elucidate the influence of stearic acid on the wettability, the water contact angles for UiO-66(Zr)-green and 10SA/UiO-66(Zr) were measured (Fig. 8). In the case of 10SA/UiO-66(Zr), a contact angle of around 107.5° was recorded, while UiO-66(Zr)-green illustrated a contact angle of around 81.6°. Furthermore, the strong affinity of 10SA/UiO-66(Zr)
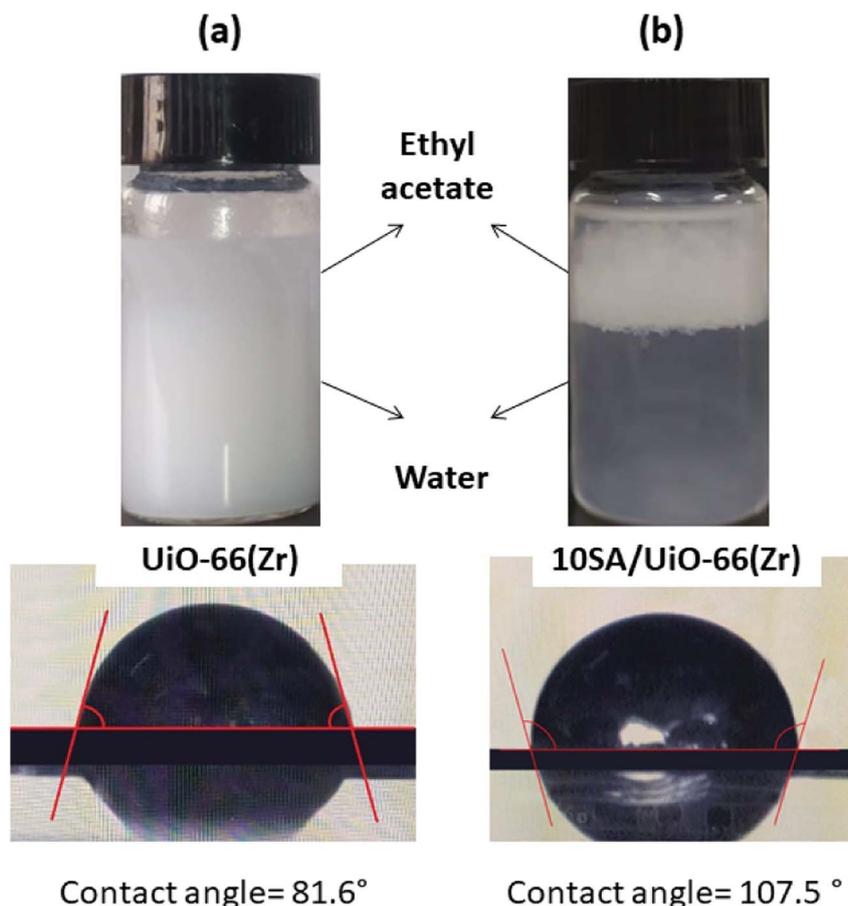


Fig. 8 Contact angles of static water over (a) UiO-66(Zr)-green and (b) 10SA/UiO-66(Zr).
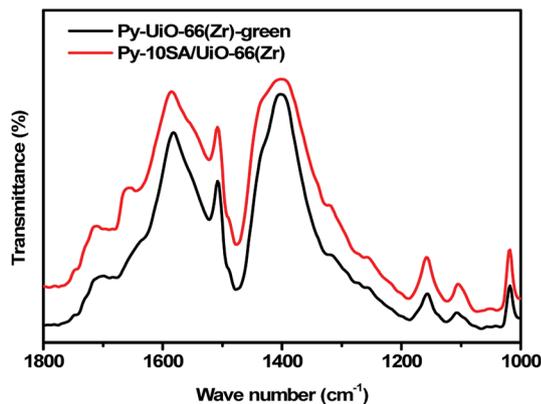
**Paper**

Fig. 9 The pyridine FT-IR spectra of UiO-66(Zr)-green and 10SA/UiO-66(Zr).



Scheme 1 Proposed scheme for the esterification of oleic acid over the 10% SA/UiO-66(Zr) catalyst.

toward the hydrophobic medium was also confirmed by the dispersion properties in two different liquid phases (water and ethyl acetate), as presented in Fig. 8. The catalysts (50 mg) were dispersed in a water–ethyl acetate (1 : 1 v/v) mixture. Most of the UiO-66(Zr)-green particles preferentially dispersed between the two phases to give a suspension (Fig. 8a). However, 10SA/UiO-66(Zr) was completely distributed in the hydrophobic ethyl acetate phase (Fig. 8b). The strong affinity for the hydrophobic phase could be assigned to the enhancement in the hydrophobicity of 10SA/UiO-66(Zr) that resulted from the introduction of stearic acid into the UiO-66(Zr) framework.
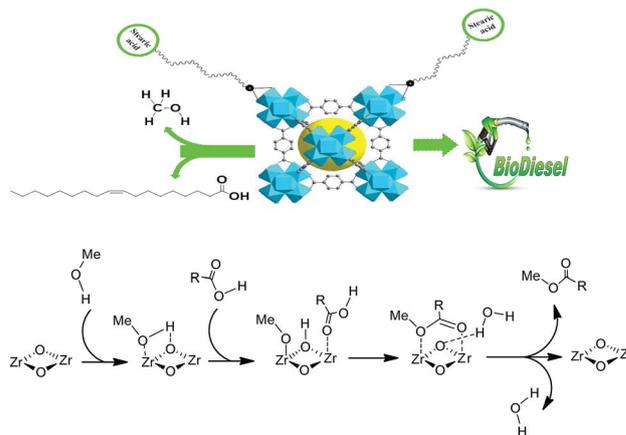
Lastly, to confirm the acidity of 10SA/UiO-66(Zr) and UiO-66(Zr)-green, we recorded the FT-IR spectra of pyridine adsorption on UiO-66(Zr)-green and 10SA/UiO-66(Zr), as depicted in Fig. 9. Fig. 9 indicates that 10SA/UiO-66(Zr) contained more acidic sites (Lewis & Bronsted acid sites) than UiO-66(Zr)-green, which could be attributed to the missing BDC linkers that connect to the Zr centers during the preparation. Further, calculations proved that 10SA/UiO-66(Zr) had a higher acid site density than UiO-66(Zr)-green (Table S1†).

All these results demonstrate the advantages that UiO-66(Zr)-green had gained by the green grafting of stearic acid in the UiO-66(Zr) network. This increases the hydrophobic environment around the zirconium active sites, enhances the acidic sites (open Zr-sites) by the absence of one or more BDC linkers during synthesis and increases the surface area and pore volume by decreasing the particle size of UiO-66(Zr).

### 3.2. Catalytic performance evaluation

Upon testing the catalytic performance of 10SA/UiO-66(Zr), UiO-66(Zr)-green and other prepared samples in the esterification reaction of oleic acid with methanol to form methyl oleate (biodiesel), as shown in Scheme 1, it was found that 10SA/UiO-66(Zr) exhibited the highest catalytic activity among these catalysts (Fig. 10).

Indeed, the superiority of 10SA/UiO-66(Zr) over UiO-66(Zr)-green and other catalysts in motivating the esterification reaction between the two different liquid phases (oleic acid and methanol) at 298 K was evident with a high yield estimated at

~94.5%, and the turnover frequency (TOF = 1.45 min$^{-1}$) was calculated according to the following eqn (6).[42]

$$\text{TOF} = \frac{X V_o \rho M_c}{W_s M_r T} \qquad (6)$$

where X, $V_o$, $M_c$, $M_r$, $W_s$, T are the conversion of the substrate, the volume (mL) of the substrate, the density (g mL$^{-1}$) of the substrate, the molar mass (g mol$^{-1}$) of the catalyst, the molar mass (g mol$^{-1}$) of the substrate, the weight (g) of the catalyst, and reaction time (min), respectively.

The pore volume of 10SA/UiO-66(Zr) was enhanced compared with that of UiO-66(Zr)-green (by about 26%) upon treatment with stearic acid (Table S2†). The enlargement in pore volume is explained in terms of the one or more missing BDC linkers, which lead to the expansion of pore volume and a slight increase in the acidity of the zirconium sites, as displayed in Fig. 9. The combination of both acidity and pore volume, beside
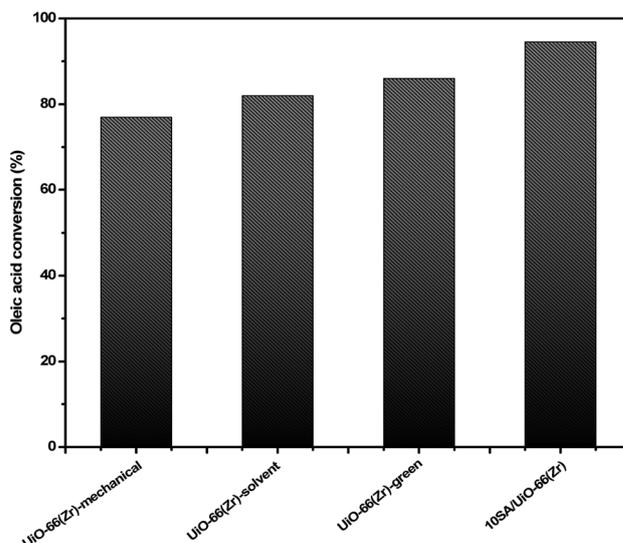


Fig. 10 Catalytic activities of the samples in the esterification reaction of oleic acid with methanol.
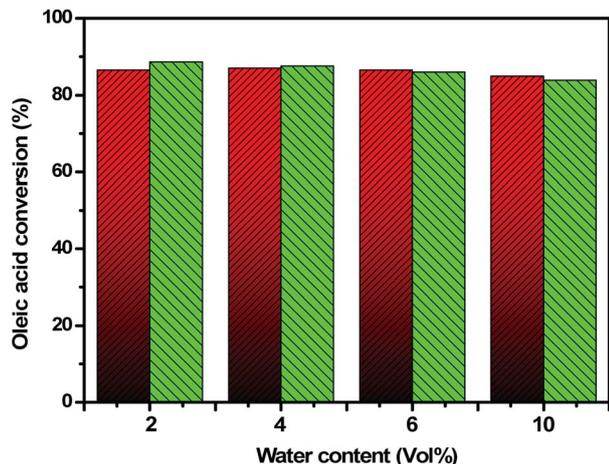
Fig. 11 Catalytic performance of 10SA/UiO-66(Zr) in the esterification of oleic acid with methanol in the presence of water at 298 K. The water content was 2–10 vol% with respect to the amount of acid. Red and green bars represent the yield after 2 h and 4 h, respectively.

the hydrophobic environment surrounding the acidic sites, apparently encourages the adsorption of reactants on the solid acid sites and facilitates the diffusion of reactants and products from the bulk solution to the surface of the solid catalyst and *vice versa*.[43,47]

### 3.3. Water tolerance of the 10SAUiO-66(Zr) catalyst

It is known that the acidic/basic sites on conventional solid acid/base catalysts are largely deactivated by water.[48] Therefore, the water tolerance test is of practical importance because it can well reflect the performance of the catalysts in biodiesel production from water-containing oil. Consequently, the impact of water content on the catalytic performance of 10SA/UiO-66(Zr) was examined in the esterification reaction of oleic acid by the addition of various volumes of water to the reaction medium at 298 K. The catalytic results are displayed in Fig. 11. The conversion over 10SA/UiO-66(Zr) reached ~94.5% within 4 h in the absence of water. But the conversion over 10SA/UiO-66(Zr) after 4 h slightly decreased with an increasing volume of water in the reaction up to 11% when a large volume of $H_2O$ (10 vol%) was utilized. This result indicates that the hydrophobic modification of UiO-66(Zr)-green by grafting stearic acid

produces an excellent solid acid catalyst not only for direct biodiesel production but also for many organic reactions that take place in an aqueous medium, such as the hydrolysis of esters.

### 3.4. Comparison of catalytic activities and adsorption capabilities

The catalytic performances of 10SA/UiO-66(Zr) and other reported homogeneous and heterogeneous acid catalysts were tested in the esterification reaction of oleic acid with methanol at 298 K, as shown in Fig. 12a. With the exception of $H_2SO_4$, which gave the same yield, the results revealed the superiority of 10SA/UiO-66(Zr) as a solid catalyst over the other reported catalysts. However, the utilization of sulfuric acid as a homogeneous acid was accompanied by high energy consumption for catalyst separation and disposal, in addition to product purification. In contrast, 10SA/UiO-66(Zr) as a heterogeneous acid catalyst could easily be separated from the reaction mixture and reused. To understand the high catalytic performance of 10SA/UiO-66(Zr) compared with other reported catalysts, such as MIL-100(Fe), UiO-66(Zr), ZMS-5, Amberlyst-15 and bentonite, the adsorption capabilities of the catalysts for oleic acid were examined, and the results are displayed in Fig. 12b. Each solid acid (0.1 g) was stirred in a mixture of oleic acid (0.05 g) and toluene (5 mL) at room temperature. After 1 h, oleic acid concentration in the solution was quantitatively analyzed by titration and gas chromatography (GC). The results revealed a high adsorption capability for 10SA/UiO-66(Zr) toward hydrophobic oleic acid due to the hydrophobic nature and microporous structure of the framework.

### 3.5. Leaching test

Generally, leaching of the active metal species into the reaction medium causes contamination of the final product and also leads to a decrease in catalyst activity. Thus, we tested the catalytic heterogeneity of the reaction by the hot filtration method.[49] The catalyst was separated from the reaction medium by filtration after 5 min (with 83% yield of methyl oleate), and the reaction was performed with the filtrate under the same reaction conditions. The results of these experiments (presented in Fig. S5†) showed that the reaction stopped with the
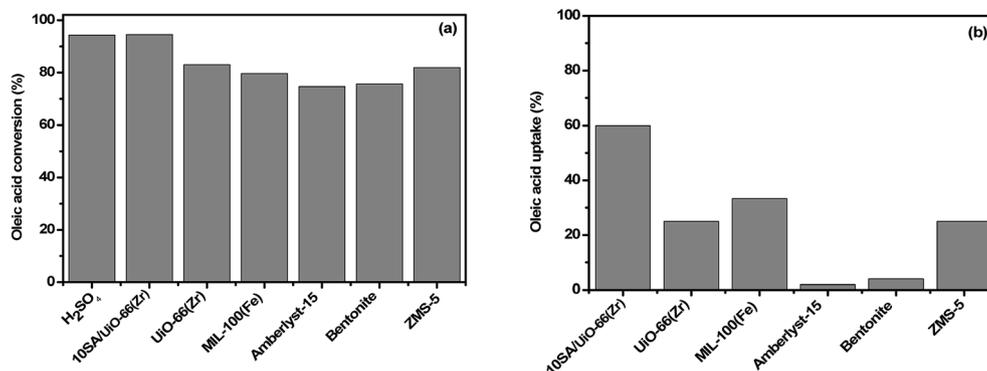


Fig. 12 Comparison of the (a) catalytic activities and (b) adsorption capabilities of 10SA/UiO-66(Zr) and other reported catalysts for oleic acid.
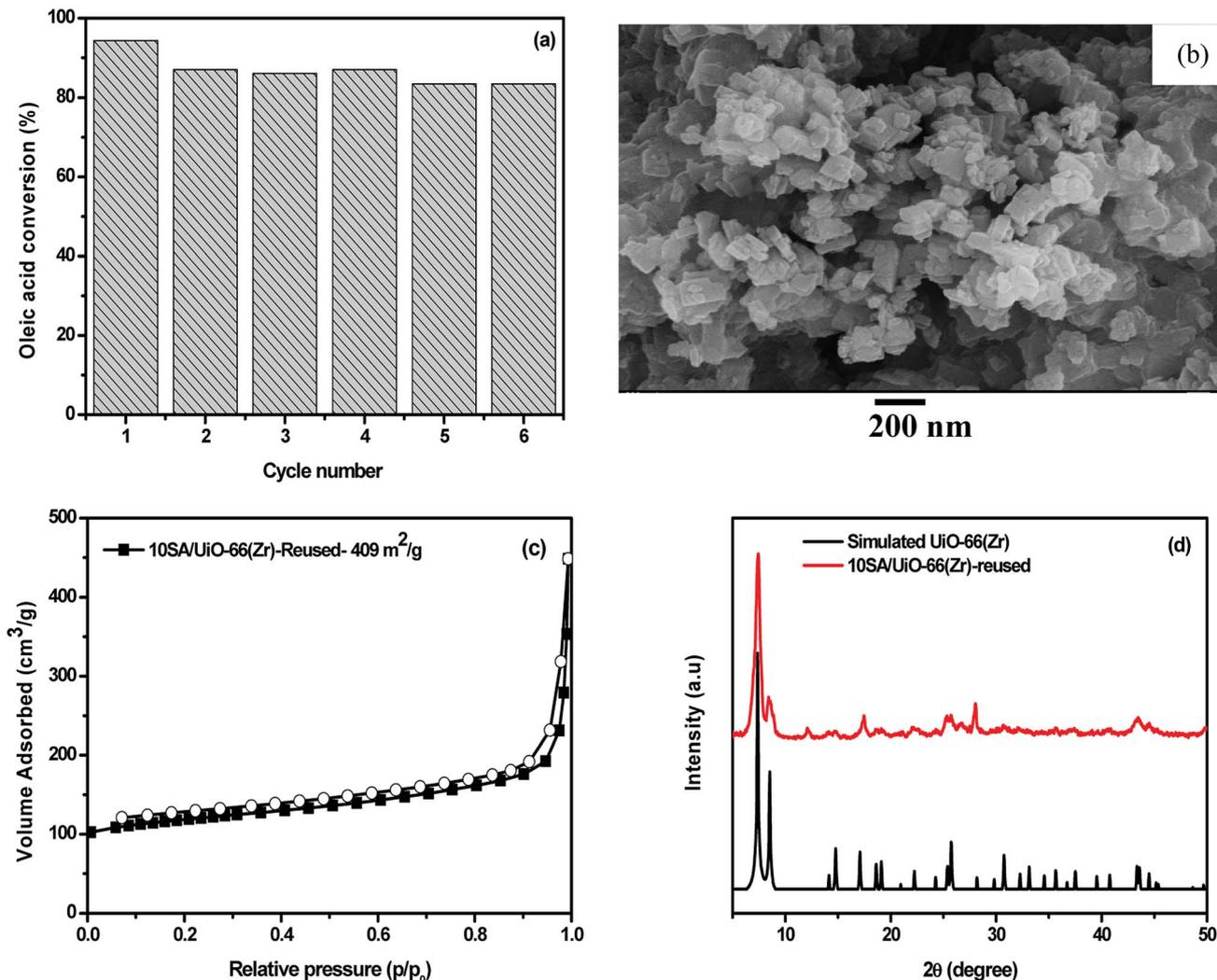
Fig. 13  (a) Reusability of 10SA/UiO-66(Zr) in the reaction of oleic acid with methanol; (b) SEM image, (c) $N_2$ sorption isotherms and (d) XRD patterns of the spent catalyst.

removal of the solid catalyst (10SA/UiO-66(Zr)). These results demonstrated that the catalytic system did not behave like a homogeneous system.

### 3.6.   Catalyst reusability

Since cost is the major concern in biodiesel production, the development of recyclable solid catalysts has gained great attention for ease of separation, low cost and lower environmental problems. The recyclability of 10SA/UiO-66(Zr) was evaluated in the esterification reaction of oleic acid with methanol at 298 K. After each cycle, the catalyst was separated and rinsed with methanol three times to remove adsorbed oleic acid. Then, the product was dried and activated for 6 h at 150 °C for the next cycle. As displayed in Fig. 13a, the yield after six cycles was maintained above 83%. These results indicated that the catalyst can be reused with no significant loss of activity. To detect the structural stability of 10SA/UiO-66(Zr), the porosity, crystallinity and surface morphology of the spent catalyst were also examined (Fig. 13). The result indicated that 10SA/UiO-

66(Zr) could almost maintain the structural properties after reuse, suggesting that 10SA/UiO-66(Zr) was stable. Undoubtedly, the adsorption of unreacted oleic acid and products on the catalyst surface led to a decrease in surface area (Fig. 13c). Furthermore, the FT-IR results (Fig. S4†) of the spent catalysts showed two sharp absorption bands at 2855 cm$^{-1}$ and 2960 cm$^{-1}$ assigned to the symmetric and asymmetric –CH$_2$ stretching vibrations from oleic acid, respectively, suggesting that unreacted oleic acid might be adsorbed onto the surface of the catalysts and could block the active sites.

### 3.7.   Kinetic study of the esterification reaction over 10SA/ UiO-66(Zr)

The kinetic behavior of 10SA/UiO-66(Zr) in the esterification reaction of oleic acid was studied under the optimum conditions of 6 wt% catalyst loading and oleic acid to methanol molar ratio of 1 : 39 in the temperature range of 298–353 K (Fig. 14). The conversion of oleic acid increased with the reaction
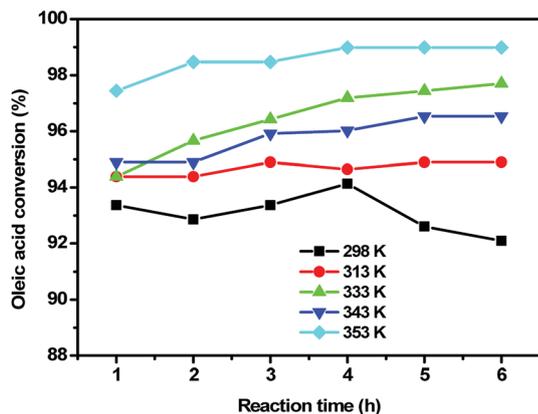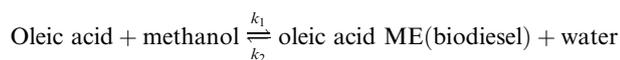
**Fig. 14** The effect of reaction temperature on the conversion of oleic acid over the 10SA/UiO-66(Zr) catalyst under optimized reaction conditions.

temperature.[50,51] The overall reaction is depicted in the following equation:

$$\text{Oleic acid} + \text{methanol} \underset{k_2}{\overset{k_1}{\rightleftharpoons}} \text{oleic acid ME(biodiesel)} + \text{water}$$

The overall reaction rate $(r_A)$ was evaluated based on the following equations:

$$r_A = -(dC_A/dt) = kC_A{}^n \tag{7}$$

$$C_A = C_{A0}(1 - x) \tag{8}$$

where $C_{A_0}$ and $x$ are the initial concentration and conversion of oleic acid, respectively. Thus, the integration of the above equation for concentration $C_A$ with regard to time $t$ gives the rate constant $k$ of the $n$th order, as shown in eqn (9).

$$\ln(1 - x) = kt \tag{9}$$

The activation energy was estimated from the plot of $(\ln k)$ against $(1/T)$, as derived from the Arrhenius equation:

$$k = Ae^{(-E_a/RT)} \tag{10}$$

where $E_a$ is the activation energy, $A$ is the frequency factor, $R$ is the universal gas constant, and $T$ is the absolute temperature. Fig. 15 illustrates the linear relationship between $-\ln(1 - x)$ and time at different reaction temperatures (Fig. 15a) and the Arrhenius plot of $(\ln k)$ versus $(1/T)$ (Fig. 15b). This plot gives a straight line with a slope of $(E_a/R)$ and an intercept of $(\ln A)$. Table 1 elucidates an increase in the rate constant with rising temperature.[52]

The derived activation energy over 10SA/UiO-66(Zr) was 32.53 kJ mol$^{-1}$, which is lower than the previously reported values (46.69 and 50.74 kJ mol$^{-1}$).[53,54] This result clarifies the vital role of the combining effect of hydrophobicity, acidity and pore volume in enhancing the rate of the methanolysis of oleic acid by decreasing the energy barrier $(E_a)$. Furthermore, the activation energy value confirmed that the esterification
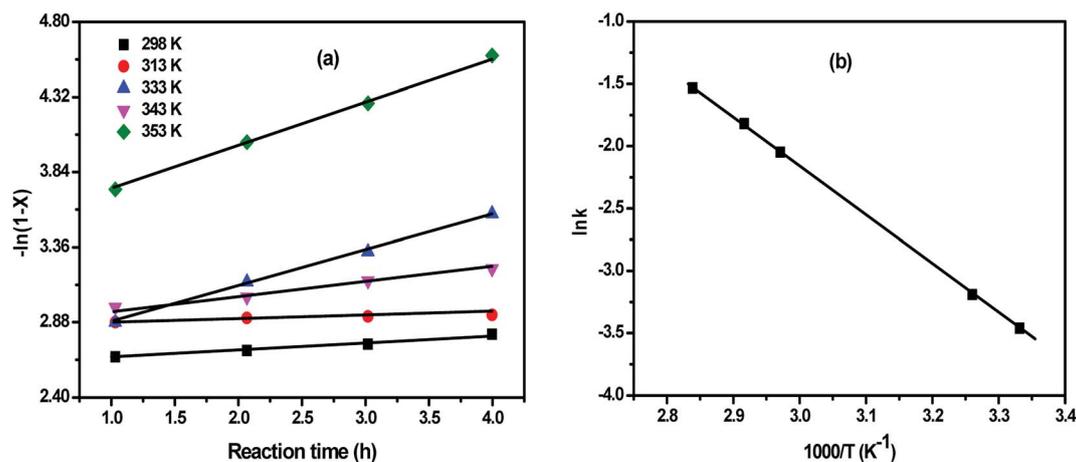


**Fig. 15** (a) The linear relationship between $-\ln(1 - x)$ vs. $t$ at different temperatures; (b) Arrhenius plot of $\ln k$ vs. $1/T$.

**Table 1** Temperature dependency of the rate constant and calculated activation energy

| Temp. (K) | Order of the reaction $(n)$ | Rate constant $k$ (h$^{-1}$) | Activation energy $(E_a)$ (kJ mol$^{-1}$ K$^{-1}$) | Frequency factor $(A \times 10^{-5})$ |
|---|---|---|---|---|
| 298 | 0.9945 | 0.0441 | 32.53 | 6.45 |
| 313 | 0.9973 | 0.0235 | | |
| 333 | 1.0135 | 0.2288 | | |
| 343 | 1.0000 | 0.0976 | | |
| 353 | 1.0104 | 0.2753 | | |

reaction was kinetically controlled not diffusively controlled.[54] This suggests that the esterification reaction over 10SA/UiO-66(Zr) was chemically controlled and not by diffusion or mass transfer limitations.

## 4. Conclusions

In short, grafting of stearic acid on UiO-66(Zr) by a facile route increased the hydrophobicity of the framework. The enhancement in hydrophobicity encourages the adsorption of oleophilic material (oleic acid) and prevents the ester molecules from being hydrolyzed back into the reactant by desorption of the hydrophilic material (water) on the surface. Further, the surface area and pore volume of UiO-66(Zr) greatly increased on decreasing the particle size. These merits are important in catalyzing the esterification reaction of oleic acid at 298 K to produce biodiesel. Moreover, the catalyst could still maintain high conversion when the reaction was carried out in the presence of different quantities of water, which confirms the role of the hydrophobic character acquired by grafting stearic acid in UiO-66(Zr). Furthermore, 10SA/UiO-66(Zr) exhibited excellent reusability with negligible changes in catalyst characteristics. This synthetic strategy provides a new and green route to prepare MOFs with enhanced hydrophobicity for catalyzing various organic reactions that involve different liquid phases under mild conditions.

## Conflicts of interest

There are no conflicts to declare.

## Acknowledgements

## References

1 D. Gielen, F. Boshell, D. Saygin, M. D. Bazilian, N. Wagner and R. Gorini, The role of renewable energy in the global energy transformation, Energy Strategy Rev., 2019, 24, 38–50.

2 H.-T. Tan, K. R. Corbin and G. B. Fincher, Emerging technologies for the production of renewable liquid transport fuels from biomass sources enriched in plant cell walls, Front. Plant Sci., 2016, 7, 1854.

3 Y. Yan, X. Li, G. Wang, X. Gui, G. Li, F. Su, X. Wang and T. Liu, Biotechnological preparation of biodiesel and its high-valued derivatives: A review, Appl. Energy, 2014, 113, 1614–1631.

4 N. S. Lani, N. Ngadi, N. Y. Yahya and R. A. Rahman, Synthesis, characterization and performance of silica impregnated calcium oxide as heterogeneous catalyst in biodiesel production, J. Clean. Prod., 2017, 146, 116–124.

5 J. Nisar, R. Razaq, M. Farooq, M. Iqbal, R. A. Khan, M. Sayed, A. Shah and I. ur Rahman, Enhanced biodiesel production from Jatropha oil using calcined waste animal bones as catalyst, Renew. Energy, 2017, 101, 111–119.

6 K. Prueksakorn and S. H. Gheewala, Full chain energy analysis of biodiesel from Jatropha curcas L. in Thailand, Environ. Sci. Technol., 2008, 42, 3388–3393.

7 E. Aransiola, T. Ojumu, O. Oyekola, T. Madzimbamuto and D. Ikhu-Omoregbe, A review of current technology for biodiesel production: state of the art, Biomass Bioenergy, 2014, 61, 276–297.

8 A. M. El-Nahas, T. A. Salaheldin, T. Zaki, H. H. El-Maghrabi, A. M. Marie, S. M. Morsy and N. K. Allam, Functionalized cellulose-magnetite nanocomposite catalysts for efficient biodiesel production, Chem. Eng. J., 2017, 322, 167–180.

9 J. A. Khan, Y. Jamal, A. Shahid and B. O. N. Boulanger, Esterification of acetic and oleic acids within the Amberlyst 15 packed catalytic column, Korean J. Chem. Eng., 2016, 33, 582–586.

10 M. Sarno and M. Iuliano, Biodiesel production from waste cooking oil, Green Process. Synth., 2019, 8, 828–836.

11 M. Farooq, A. Ramli and D. Subbarao, Biodiesel production from waste cooking oil using bifunctional heterogeneous solid catalysts, J. Clean. Prod., 2013, 59, 131–140.

12 A. Islam, Y. H. Taufiq-Yap, E.-S. Chan, M. Moniruzzaman, S. Islam and M. N. Nabi, Advances in solid-catalytic and non-catalytic technologies for biodiesel production, Energy Convers. Manag., 2014, 88, 1200–1218.

13 F. Guo, Z. Fang, C. C. Xu and R. L. Smith Jr, Solid acid mediated hydrolysis of biomass for producing biofuels, Prog. Energy Combust. Sci., 2012, 38, 672–690.

14 W. Thitsartarn and S. Kawi, An active and stable CaO–CeO₂ catalyst for transesterification of oil to biodiesel, Green Chem., 2011, 13, 3423–3430.

15 N. Jalilnejad Falizi, T. Güngören Madenoğlu, M. Yüksel and N. Kabay, Biodiesel production using gel-type cation exchange resin at different ionic forms, Int. J. Energy Res., 2019, 43, 2188–2199.

16 V. Kampars, Z. Abelniece and S. Blaua, The Unanticipated Catalytic Activity of Lithium tert-Butoxide/THF in the Interesterification of Rapeseed Oil with Methyl Acetate, J. Chem., 2019, 2019, 1509706.

17 K. J. Viner, H. M. Roy, R. Lee, O. He, P. Champagne and P. G. Jessop, Transesterification of soybean oil using a switchable-hydrophilicity solvent, 2-(dibutylamino) ethanol, Green Chem., 2019, 21, 4786–4791.

18 Q. Liu, B. Wang, C. Wang, Z. Tian, W. Qu, H. Ma and R. Xu, Basicities and transesterification activities of Zn–Al hydrotalcites-derived solid bases, Green Chem., 2014, 16, 2604–2613.

19 I. M. Firdaus, T. Fitriany, M. N. Hidayah, A. Soleh, K. H. Pratama and F. Febiyanto, Use of Mg-Al/hydrotalcite Catalyst in Biodiesel Production from Avocado Seed Oils: A Preliminary Study, J. Kim. Ter. Indones., 2019, 21, 45–54.

20 C.-Y. Zhang, W.-L. Shao, W.-X. Zhou, Y. Liu, Y.-Y. Han, Y. Zheng and Y.-J. Liu, Biodiesel Production by Esterification Reaction on K+ Modified MgAl-Hydrotalcites Catalysts, Catalysts, 2019, 9, 742.

21 A. S. Bharadwaj, M. Singh, S. Niju, K. M. S. Begum and N. Anantharaman, Biodiesel production from rubber seed oil using calcium oxide derived from eggshell as catalyst–optimization and modeling studies, *Green Process. Synth.*, 2019, **8**, 430–442.

22 N. Gutiérrez-Ortega, E. Ramos-Ramírez, A. Serafín-Muñoz, A. Zamorategui-Molina and J. Monjaraz-Vallejo, Use of Co/Fe-Mixed Oxides as Heterogeneous Catalysts in Obtaining Biodiesel, *Catalysts*, 2019, **9**, 403.

23 J. Toledo Arana, J. J. Torres, D. F. Acevedo, C. O. Illanes, N. A. Ochoa and C. L. Pagliero, One-Step Synthesis of CaO-ZnO Efficient Catalyst for Biodiesel Production, *Int. J. Chem. Eng.*, 2019, **2019**, 1806017.

24 A. Buasri, K. Rochanakit, W. Wongvitvichot, U. Masa-ard and V. Loryuenyong, The application of calcium oxide and magnesium oxide from natural dolomitic rock for biodiesel synthesis, *Energy Procedia*, 2015, **79**, 562–566.

25 D. A. Kamel, H. A. Farag, N. K. Amin, A. A. Zatout and R. M. Ali, Smart utilization of jatropha (Jatropha curcas Linnaeus) seeds for biodiesel production: optimization and mechanism, *Ind. Crop. Prod.*, 2018, **111**, 407–413.

26 K. Fukuhara, K. Nakajima, M. Kitano, S. Hayashi and M. Hara, Transesterification of Triolein over hydrophobic microporous carbon with $SO_3H$ groups, *ChemCatChem*, 2015, **7**, 3945–3950.

27 F. Liu, W. Kong, C. Qi, L. Zhu and F.-S. Xiao, Design and synthesis of mesoporous polymer-based solid acid catalysts with excellent hydrophobicity and extraordinary catalytic activity, *ACS Catal.*, 2012, **2**, 565–572.

28 F. Liu, X. Meng, Y. Zhang, L. Ren, F. Nawaz and F.-S. Xiao, Efficient and stable solid acid catalysts synthesized from sulfonation of swelling mesoporous polydivinylbenzenes, *J. Catal.*, 2010, **271**, 52–58.

29 F. Liu, K. Huang, A. Zheng, F.-S. Xiao and S. Dai, Hydrophobic solid acids and their catalytic applications in green and sustainable chemistry, *ACS Catal.*, 2017, **8**, 372–391.

30 K. Nakajima, R. Noma, M. Kitano and M. Hara, Titania as an early transition metal oxide with a high density of Lewis acid sites workable in water, *J. Phys. Chem. C*, 2013, **117**, 16028–16033.

31 Y. Bai, Y. Dou, L.-H. Xie, W. Rutledge, J.-R. Li and H.-C. Zhou, Zr-based metal–organic frameworks: design, synthesis, structure, and applications, *Chem. Soc. Rev.*, 2016, **45**, 2327–2367.

32 K. Leus, T. Bogaerts, J. De Decker, H. Depauw, K. Hendrickx, H. Vrielinck, V. Van Speybroeck and P. Van Der Voort, Systematic study of the chemical and hydrothermal stability of selected "stable" metal organic frameworks, *Microporous Mesoporous Mater.*, 2016, **226**, 110–116.

33 C. Caratelli, J. Hajek, F. G. Cirujano, M. Waroquier, F. X. L. i. Xamena and V. Van Speybroeck, Nature of active sites on UiO-66 and beneficial influence of water in the catalysis of Fischer esterification, *J. Catal.*, 2017, **352**, 401–414.

34 J. Canivet, M. Vandichel and D. Farrusseng, Origin of highly active metal–organic framework catalysts: defects? Defects!, *Dalton Trans.*, 2016, **45**, 4090–4099.

35 Y. Liu, R. C. Klet, J. T. Hupp and O. Farha, Probing the correlations between the defects in metal–organic frameworks and their catalytic activity by an epoxide ring-opening reaction, *Chem. Commun.*, 2016, **52**, 7806–7809.

36 X. Liang, M. Zeng and C. Qi, One-step synthesis of carbon functionalized with sulfonic acid groups using hydrothermal carbonization, *Carbon*, 2010, **48**, 1844–1848.

37 X. Liang and J. Yang, Synthesis of a novel carbon based strong acid catalyst through hydrothermal carbonization, *Catal. Lett.*, 2009, **132**, 460.

38 F. Liu, L. Wang, Q. Sun, L. Zhu, X. Meng and F.-S. Xiao, Transesterification catalyzed by ionic liquids on superhydrophobic mesoporous polymers: heterogeneous catalysts that are faster than homogeneous catalysts, *J. Am. Chem. Soc.*, 2012, **134**, 16948–16950.

39 X. Chen, P. Qian, T. Zhang, Z. Xu, C. Fang, X. Xu, W. Chen, P. Wu, Y. Shen and S. Li, Catalyst surfaces with tunable hydrophilicity and hydrophobicity: metal–organic frameworks toward controllable catalytic selectivity, *Chem. Commun.*, 2018, **54**, 3936–3939.

40 Y. Hu, L. Dai, D. Liu and W. Du, Rationally designing hydrophobic UiO-66 support for the enhanced enzymatic performance of immobilized lipase, *Green Chem.*, 2018, **20**, 4500–4506.

41 G. Ye, D. Zhang, X. Li, K. Leng, W. Zhang, J. Ma, Y. Sun, W. Xu and S. Ma, Boosting Catalytic Performance of Metal–Organic Framework by Increasing the Defects via a Facile and Green Approach, *ACS Appl. Mater. Interfaces*, 2017, **9**, 34937–34943.

42 A. S. Abou-Elyazed, G. Ye, Y. Sun and A. M. El-Nahas, A Series of UiO-66 (Zr)-Structured Materials with Defects as Heterogeneous Catalysts for Biodiesel Production, *Ind. Eng. Chem. Res.*, 2019, **58**, 21961–21971.

43 A. I. Osman, J. K. Abu-Dahrieh, D. W. Rooney, S. A. Halawy, M. A. Mohamed and A. Abdelkader, Effect of precursor on the performance of alumina for the dehydration of methanol to dimethyl ether, *Appl. Catal., B*, 2012, **127**, 307–315.

44 X. Shi, R. Rosa and A. Lazzeri, On the coating of precipitated calcium carbonate with stearic acid in aqueous medium, *Langmuir*, 2010, **26**, 8474–8482.

45 Y.-X. Zeng, X.-W. Zhong, Z.-Q. Liu, S. Chen and N. Li, Preparation and enhancement of thermal conductivity of heat transfer oil-based $MoS_2$ nanofluids, *J. Nanomater.*, 2013, **2013**, 1–6.

46 J. H. Cavka, S. Jakobsen, U. Olsbye, N. Guillou, C. Lamberti, S. Bordiga and K. P. Lillerud, A new zirconium inorganic building brick forming metal organic frameworks with exceptional stability, *J. Am. Chem. Soc.*, 2008, **130**, 13850–13851.

47 E. G. Fawaz, D. A. Salam, L. Pinard and T. J. Daou, Study on the catalytic performance of different crystal morphologies of HZSM-5 zeolites for the production of biodiesel:

a strategy to increase catalyst effectiveness, *Catal. Sci. Technol.*, 2019, **9**, 5456–5471.

48 M. D. Argyle and C. H. Bartholomew, Heterogeneous catalyst deactivation and regeneration: a review, *Catalysts*, 2015, **5**, 145–269.

49 M. Lamblin, L. Nassar-Hardy, J. C. Hierso, E. Fouquet and F. X. Felpin, Recyclable heterogeneous palladium catalysts in pure water: Sustainable developments in Suzuki, Heck, Sonogashira and Tsuji–Trost reactions, *Adv. Synth. Catal.*, 2010, **352**, 33–79.

50 A. L. Cardoso, S. C. G. Neves and M. J. Da Silva, Esterification of oleic acid for biodiesel production catalyzed by SnCl$_2$: a kinetic investigation, *Energies*, 2008, **1**, 79–92.

51 M. Mandake, S. Anekar and S. Walke, Kinetic study of catalyzed and uncatalyzed esterification reaction of acetic acid with methanol, *American International Journal of Research in Science, Technology, Engineering & Mathematics*, 2013, **3**, 114–121.

52 Z. M. Shakoor, K. A. Sukkar and M. S. Baqer, Reaction kinetics of acetic acid and n-butanol esterification catalyzed by Dowex 50 catalyst, *Engineering and Technology Journal*, 2011, **29**, 2060–2072.

53 D. D. Suprarukmi and B. A. Sudrajat, Kinetic study on esterification of oleic acid with ultrasound assisted, *Procedia Environ. Sci*, 2015, **23**, 78–85.

54 Q. Zhang, X. Liu, T. Yang, C. Yue, Q. Pu and Y. Zhang, Facile synthesis of polyoxometalates tethered to post Fe-BTC frameworks for esterification of free fatty acids to biodiesel, *RSC Adv.*, 2019, **9**, 8113–8120.